March 1979

ANALYSIS OF WIND TUNNEL TEST RESULTS OF FLUIDIC GENERATOR FOR HIGH-ALTITUDE ROCKET

By Jonathan E. Fine

U.S. Army Electronics Research
and Development Command
Harry Diamond Laboratories
Adelphi, MD 20783

The findings in this report are not to be construed as an official Department of the Army position unless so designated by other authorized documents.

Citation of manufacturers' or trade names does not constitute an official indorsement or approval of the use thereof.

Destroy this report when it is no longer needed. Do not return it to the originator.

UNCLASSIFIED

SECURITY CLASSIFICATION OF THIS PAGE *(When Data Entered)*

REPORT DOCUMENTATION PAGE		READ INSTRUCTIONS BEFORE COMPLETING FORM
1. REPORT NUMBER HDL-TR-1877	2. GOVT ACCESSION NO.	3. RECIPIENT'S CATALOG NUMBER
4. TITLE *(and Subtitle)* Analysis of Wind Tunnel Test Results of Fluidic Generator for High-Altitude Rocket		5. TYPE OF REPORT & PERIOD COVERED Technical Report 6. PERFORMING ORG. REPORT NUMBER
7. AUTHOR(s) Jonathan E. Fine		8. CONTRACT OR GRANT NUMBER(s)
9. PERFORMING ORGANIZATION NAME AND ADDRESS Harry Diamond Laboratories 2800 Powder Mill Road Adelphi, MD 20783		10. PROGRAM ELEMENT, PROJECT, TASK AREA & WORK UNIT NUMBERS Program Ele: 6.33.03.A
11. CONTROLLING OFFICE NAME AND ADDRESS U.S. Army Materiel Development and Readiness Command Alexandria, VA 22333		12. REPORT DATE March 1979 13. NUMBER OF PAGES 31
14. MONITORING AGENCY NAME & ADDRESS*(if different from Controlling Office)*		15. SECURITY CLASS. *(of this report)* UNCLASSIFIED 15a. DECLASSIFICATION/DOWNGRADING SCHEDULE

16. DISTRIBUTION STATEMENT *(of this Report)*

Approved for public release; distribution unlimited.

17. DISTRIBUTION STATEMENT *(of the abstract entered in Block 20, if different from Report)*

18. SUPPLEMENTARY NOTES

HDL Project: 424894
DRCMS Code: 6433035640012
DA: 1X463303D564

19. KEY WORDS *(Continue on reverse side if necessary and identify by block number)*

Air-driven generator	Safety and arming
Power supply	Environmental signature
Battery	Fluidic generator
Rocket fuze	

20. ABSTRACT *(Continue on reverse side if necessary and identify by block number)*

A ram-air-driven power supply for a proposed high-altitude rocket was tested in the Naval Surface Weapons Center supersonic wind tunnel facility.

The wind tunnel data that corresponded to points on the trajectory providing the least ram-air energy showed that the generator operated throughout the test and produced a minimum

DD FORM 1 JAN 73 1473 EDITION OF 1 NOV 65 IS OBSOLETE

UNCLASSIFIED

SECURITY CLASSIFICATION OF THIS PAGE *(When Data Entered)*

20. ABSTRACT (Cont'd)

of 26.4 Vrms into a simulated fuze load near the apex where pneumatic power input is minimal.

A method of predicting generator voltage in flight from laboratory calibration data and expected flight conditions was verified for Mach numbers from 1.5 to 2.02 and free-stream total pressures of up to 20 lb/in.^{2} abs (137 kPa).

CONTENTS

FIGURES

FIGURES (Cont'd)

TABLE

1. INTRODUCTION

Tests were conducted at the Naval Surface Weapons Center (NSWC, White Oak, MD, Laboratories) supersonic wind tunnel facility on 19 and 20 July 1977 to determine the output characteristics of a ram-air-driven power supply being developed for a high-altitude rocket.

Figure 1 shows the fluidic generator power supply mounted in a fuze ogive. During flight, air enters the generator through the single entrance port in the nose and leaves through exhaust ports uniformly spaced around the circumference of the ogive. In the passage through the generator, the air vibrates a resonant chamber which transmits its oscillations through a mechanical diaphragm and rod to a reed which switches magnetic flux within a coil, thereby inducing a voltage at the coil terminals.

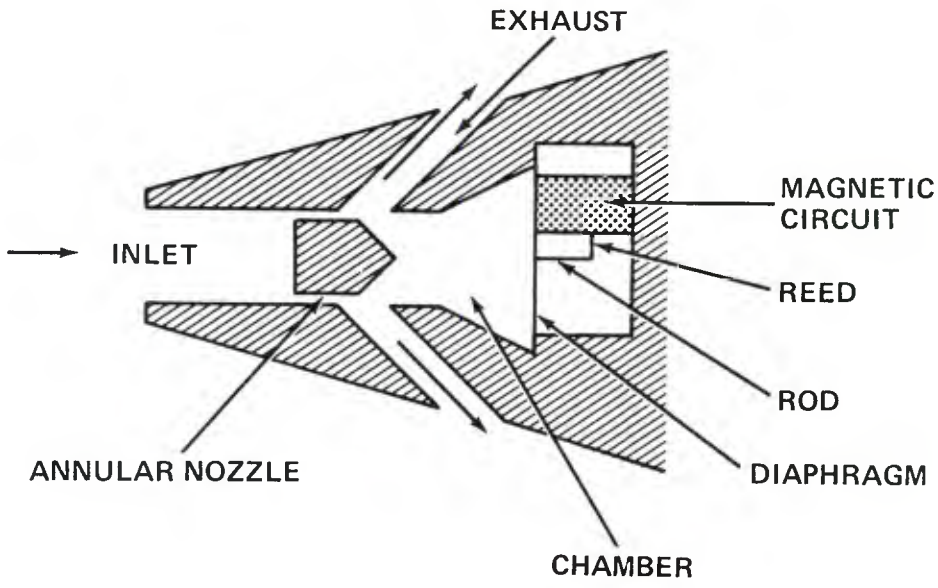

Figure 1. Air passage through ogive containing fluidic generator power supply.

The availability of ram air with sufficient energy to power the generator depends on the flight trajectories of the proposed rocket. The rocket is launched from rest or from an aircraft moving at subsonic speeds. The launch altitude varies from sea level to 10,000 ft (3048 m). Within the first second after launch, the rocket for all trajectories reaches supersonic velocity and remains in the supersonic flow regime throughout the trajectory, with flight times ranging from 30 to 120 s. Maximum flight Mach numbers of 2.75 are attained. The

wide variation in Mach number and altitude, which can be as high as 62,500 ft (19,050 m) when the rocket is launched from 10,000 ft (3048 m) causes the available pneumatic energy to the fluidic generator to vary over a wide range.

Two extremes of the flight regime are important in the design of the power supply. The first regime occurs in the high-altitude trajectory. The pneumatic energy reaches a minimum value near the apex, and a laboratory testing procedure is needed to insure that the power supply will provide sufficient voltage to the fuze load at these conditions. The second regime occurs within the first 2 s after the rocket is launched, and furnishes the most severe environment to the power supply for low-altitude launches. The pneumatic energy supplied to the generator then exceeds values that can be obtained in the laboratory or in the wind tunnel; hence, field tests are needed in this regime to verify the structural integrity and voltage output of the power supply.

This report is divided into two sections. In the first section, the wind tunnel data are used to infer the operation of the fluidic generator near the apex of the high-altitude trajectory where pneumatic energy is a minimum. The only data used are from portions of the wind tunnel profiles that correspond to conditions expected in flight along the trajectory. In the second section of this report, an analysis is made to relate laboratory data to the flight conditions near the apex and thus to furnish a method of predicting the generator output for the high-altitude portion of any flight profile. More extensive use is made of the wind tunnel data to verify the method, even though the data do not always correspond to expected trajectory points.

2. EVALUATION OF FLUIDIC GENERATOR OUTPUT NEAR APEX OF HIGH-ALTITUDE TRAJECTORY

The purpose of this section is to use data from the wind tunnel test to infer the operation of the fluidic generator in flight near the apex of the trajectory that furnishes the least pneumatic input power to the generator.

2.1 Relationship of Trajectory to Wind Tunnel Profile

The rocket high-altitude trajectory (to be partially simulated in the wind tunnel) is shown in figure 2, in which altitude is plotted versus horizontal range. The flight Mach (M) number and total pressure are indicated at various points. Near apex, the rocket achieves a minimum altitude of 62,500 ft (19,050 m) and minimum M = 1.39. Figure 3 shows the trajectory plotted in terms of the wind tunnel parameters of Mach number versus altitude. The Mach number range of the trajectory is from 1.39 to 2.72, and the altitude varies from 10,000 ft at firing to 62,500 ft at apex (from 3048 to 19,050 m).

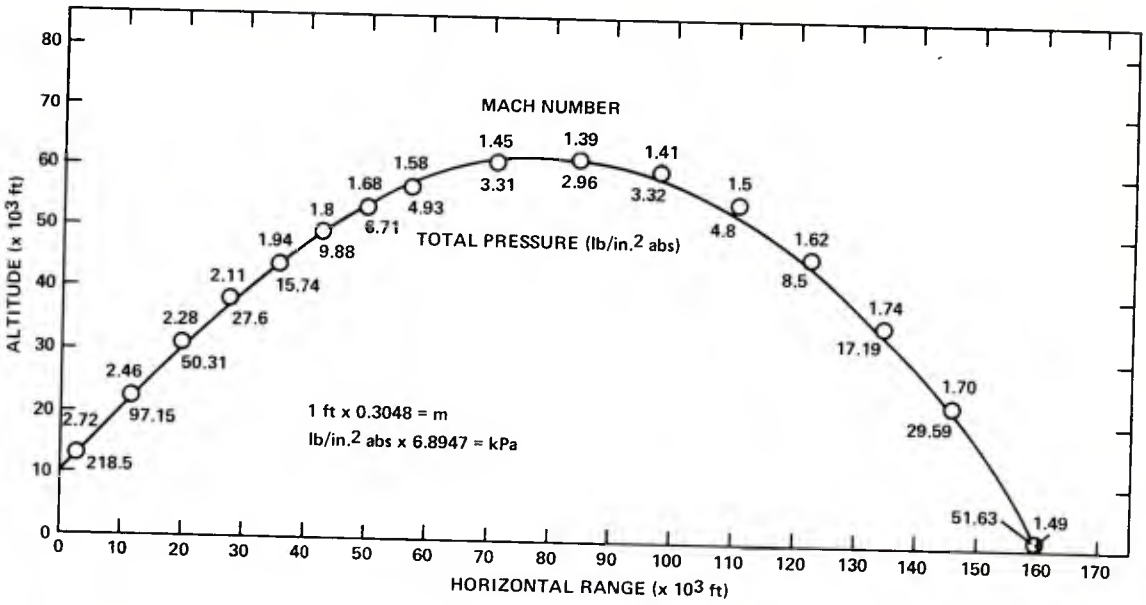

Figure 2. High-altitude trajectory (quadrant elevation = 50 deg, firing altitude = 10,000 ft).

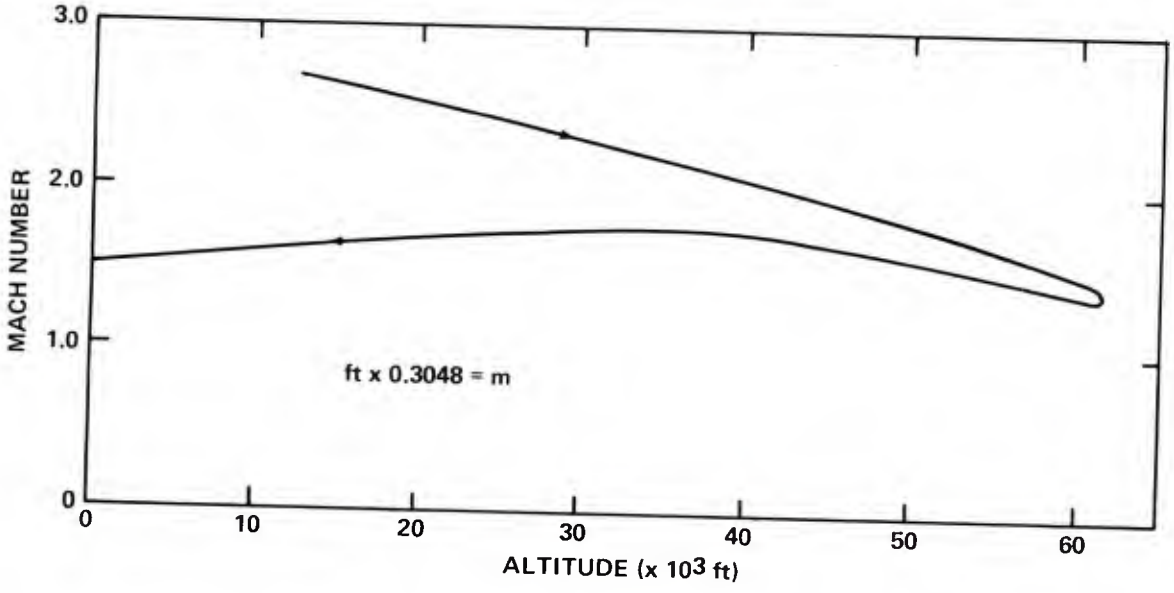

Figure 3. Variation of Mach number with altitude on trajectory (quadrant elevation = 50 deg, initial altitude = 10,000 ft).

Figure 4 shows the conditions attainable in the wind tunnel on a plot of Mach number versus altitude. The conditions fall along lines of constant Mach number, which correspond to the four fixed nozzle blocks available for use in the tunnel.

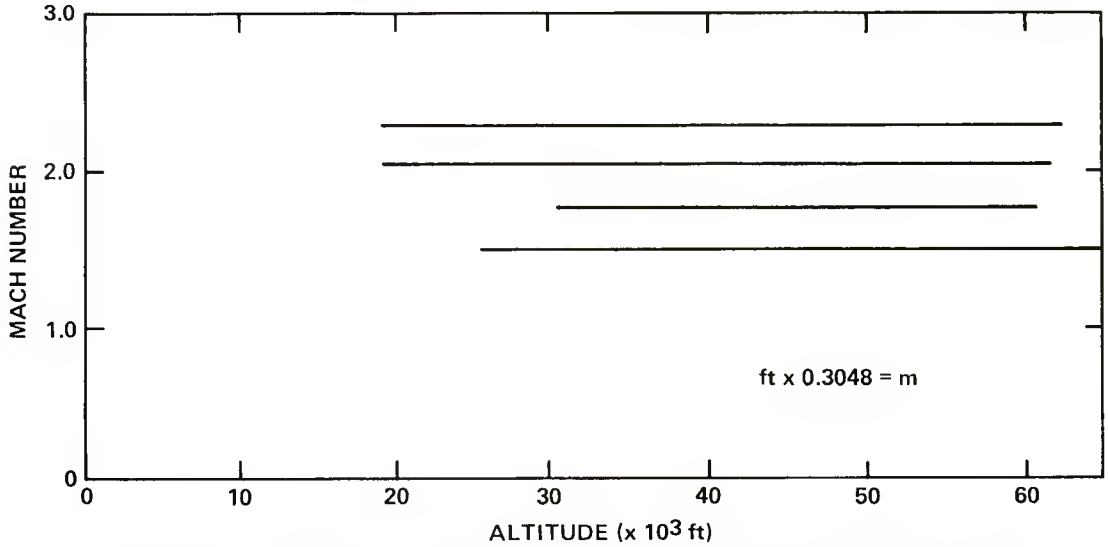

Figure 4. Conditions of Mach number and altitude obtainable in wind tunnel.

When the curves on figures 3 and 4 are plotted on the same graph, the points of intersection (indicated by "x") are the tunnel conditions that correspond to the indicated points along the trajectory (fig. 5).

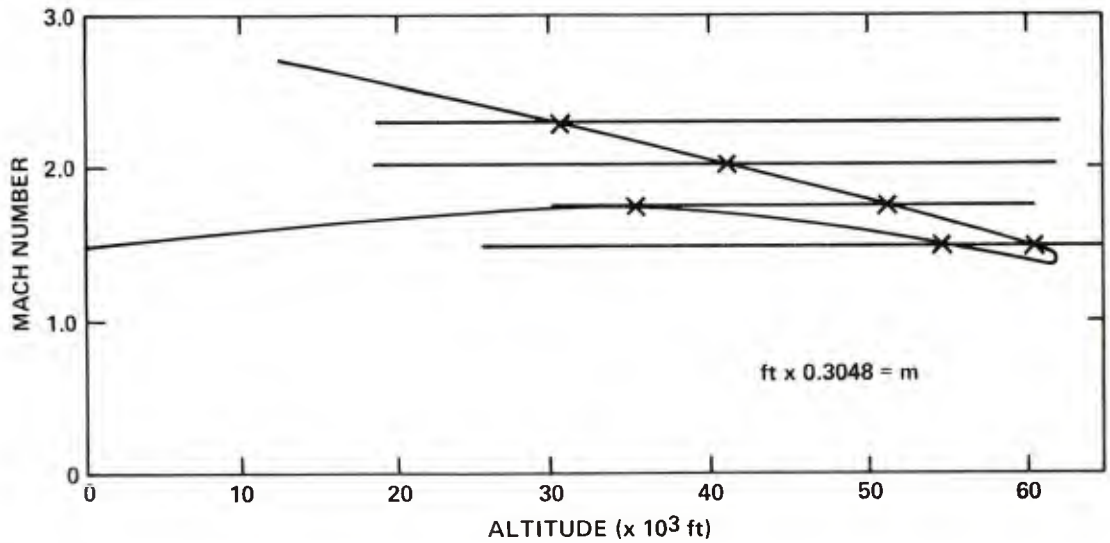

Figure 5. Trajectory conditions obtainable in wind tunnel.

2.2 Hardware and Test Procedure

For the tests, a reed-type fluidic generator was placed inside an ogive and mounted on a sting within the wind tunnel (fig. 6). During the tunnel tests, ram air enters the generator through a 0.5-in.-diam (12.7-mm) opening in the ogive nose, and exhausts through 24 orifices of 0.106-in.-diam (2.7 mm) uniformly spaced around the circumference of the ogive. The electrical output supplied to an equivalent fuze circuit is monitored from leads brought from the generator out of the tunnel through the sting. The equivalent fuze load is a 0.03-μF capacitor in series with a 2.5-kohm resistor.

During the wind tunnel test, total pressure, total temperature, and generator voltage were monitored. The Mach number was established by the nozzle block used. The altitude was then computed in terms of the total pressure, temperature, and Mach number.

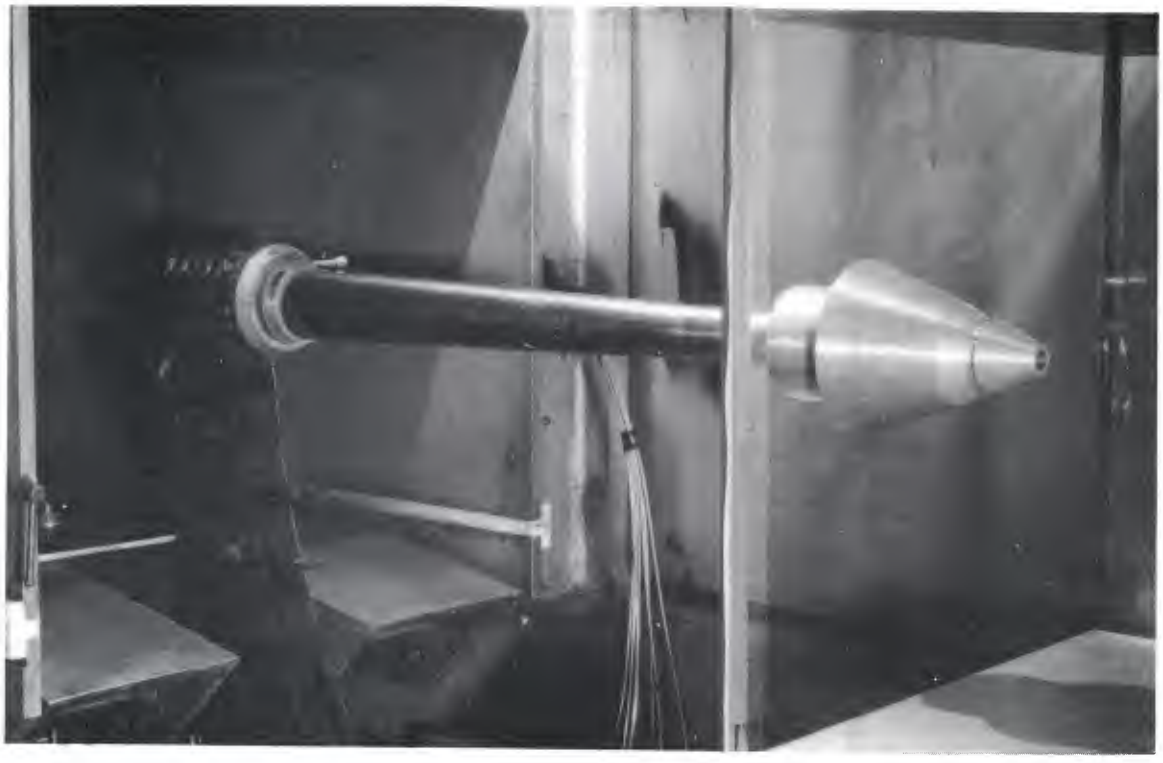

Figure 6. Ogive mounted in wind tunnel.

2.3 Test Results and Conclusions

The voltage generated at each of the trajectory conditions is shown in table I. These points are also plotted on the high-altitude trajectory in figure 7.

TABLE I. FLUIDIC GENERATOR OUTPUT AT POINTS ON HIGH-ALTITUDE TRAJECTORY

Mach No.	Altitude (1000 ft)[a]	Equivalent load voltage (ac, rms)
2.3	30.5	109
2.02	41.0	78.7
1.76	51.3	49.2
1.50	60.5	33.5
1.50	54.7	35.4
1.76	35.0	74.7

[a] *ft × 0.3048 = m*

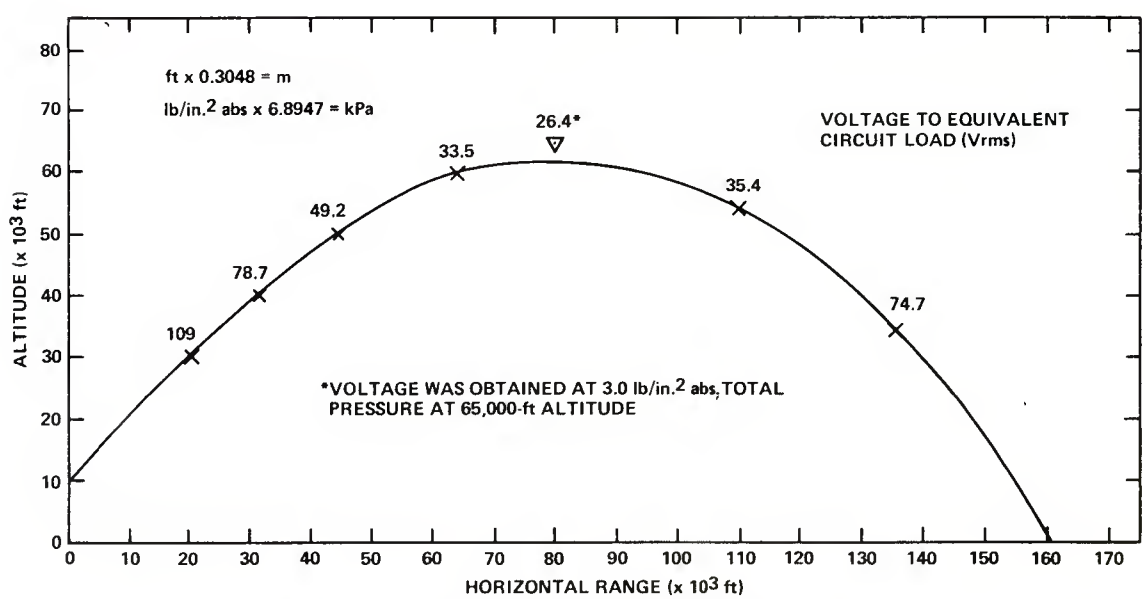

Figure 7. Fluidic generator output voltage measured in wind tunnel at points of high-altitude trajectory.

It is apparent from figure 5 that the conditions of altitude and Mach number at the apex cannot be fully simulated with the Mach 1.5 nozzle. The total pressure at the apex is 3 lb/in.^{2} abs (20.68 kPa) at Mach 1.39 (fig. 2). The total pressure of 3 lb/in.^{2} abs at the apex can be obtained by operating the tunnel at an altitude of 65,000 ft (19,812 m) even though the Mach 1.5 nozzle is used. The voltage value obtained at 3 lb/in.^{2} abs (20.68 kPa) Mach 1.5, and 65,000 ft (19,812 m) is 26.4 Vrms. This shows that the fluidic generator will operate over the apex of the trajectory and produce 26.4 Vrms.

The voltage and current supplied to the fuze electronics may be marginal at the apex. Further development of the generator may be required to increase the power output and insure adequate operation of the fuze at high altitudes.

In conclusion, the wind tunnel has shown that the fluidic generator operates throughout the worst-case portion of the trajectory and produces a minimum of 26.4 Vrms near apex where the available pneumatic energy is minimal.

3. METHOD OF ESTIMATING FLUIDIC GENERATOR OUTPUT IN FIELD OR IN WIND TUNNEL

This section deals with the portions of the trajectory for which the supply pressure can be simulated in the laboratory. The purpose of this study is to provide a means of measuring the output of the fluidic generator in the laboratory to estimate the output in flight along specified trajectories or in the wind tunnel under conditions in which the pneumatic energy available to the fluidic generator is a minimum.

3.1 Dependence of Generator Voltage on Supply Mass Flow Rate

The basis for this study is the observed dependence of voltage output of the fluidic generator on supply mass flow rate. The laboratory apparatus used to measure the mass flow rate is shown in figure 8. The fluidic generator is mounted within an ogive having a single inlet port at the nose and several small exhaust ports uniformly spaced around the circumference of the ogive. The ogive is clamped tightly against the settling chamber tank. The mass flow is adjusted by means of the regulator, and is determined from the flowmeter and pressure gauge readings. The electrical power at the simulated fuze circuit load is measured at each pressure setting. Typical results are shown in figure 9, in which power output is plotted versus mass flow rate for a generator in an ogive having a straight inlet. This figure shows that the generator output depends on the mass flow rate.

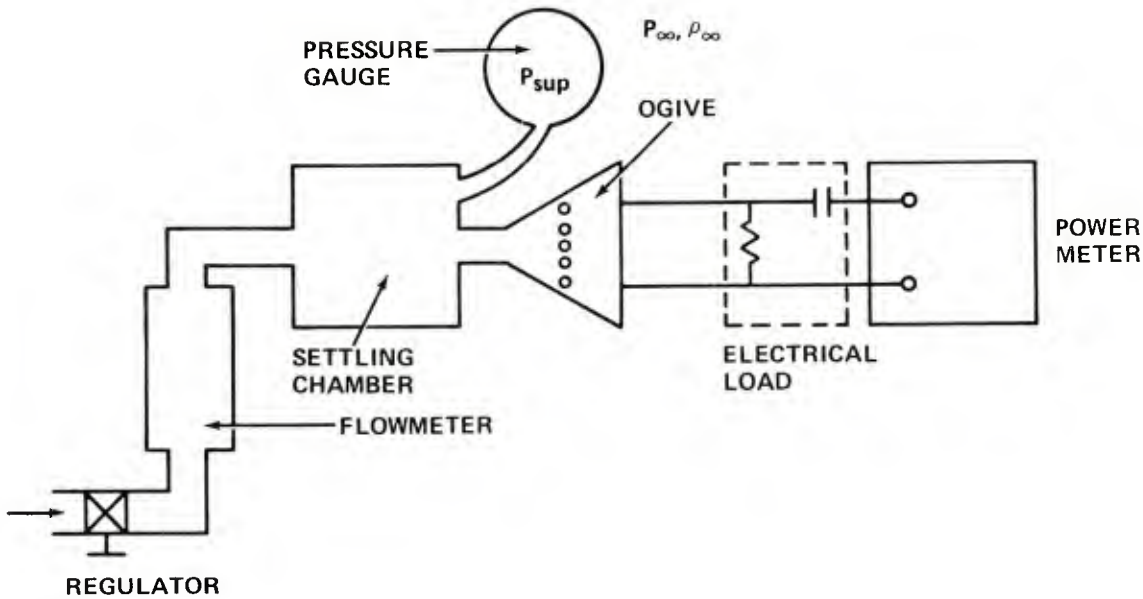

Figure 8. Laboratory apparatus for measuring fluidic generator output versus mass flow rate.

This correspondence between fluidic generator output and mass flow rate can be used to estimate the voltage available in flight. The technique is approximate, and does not require an extensive theoretical model of the behavior of the fluidic generator output on mechanical, electrical, and fluidic variables. The main assumption is that the efficiency of conversion of pneumatic to electrical energy, if not a constant, depends only on the mass flow rate. The laboratory curve of figure 9 contains the conversion efficiency implicitly, and is assumed valid for values of mass flow rate obtained from flight or wind tunnel conditions. In the following sections is developed a method of calculating the mass flow rate in flight as a function of projectile velocity, air density, and flow parameters for specified flight conditions. The expected voltage in flight is then obtained from figure 9, using the calculated mass flow rate. The effectiveness of this method can be assessed by comparing measured and predicted voltage values in the wind tunnel, where the range of variation of total pressure and altitude is greater than in the laboratory or in low quadrant elevation trajectories.

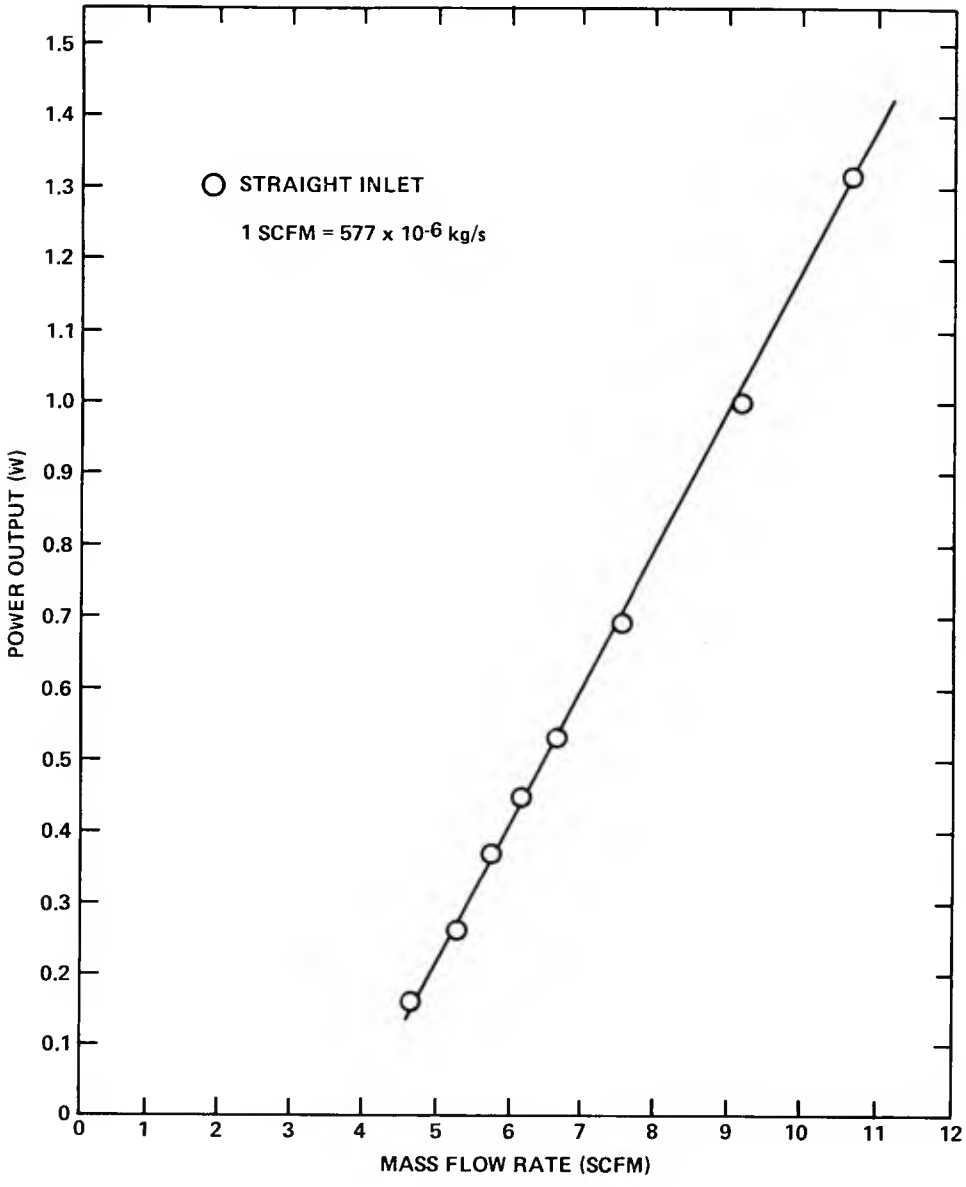

Figure 9. Fluidic generator power output versus mass flow rate in laboratory.

3.2 Theoretical Model for Estimating Mass Flow Rate

3.2.1 Flow Pattern for Flight

Although the rocket is launched from rest, it attains supersonic velocity soon after reaching a safe separation distance from the launcher, which is within 1.5 s of a 30- to 120-s flight trajectory. Thus, the portion of the trajectory over which the armed fuze is required to operate is entirely in the supersonic flow regime.

The flow patterns for supersonic portions of the flight regime of projectiles similar to the rocket being studied are described in the literature. At supersonic speeds (free-stream Mach number > 1) a bow shock wave occurs.

> The bow shock wave is curved and detached from the nose, and there is a limited region of subsonic flow between the apex of the bow wave and the body. Further downstream the flow becomes supersonic again and the conditions over the rear of the airfoil are similar to those for a sharp leading edge and an attached bow wave.[1]

This bow shock is clearly visible in a wind tunnel photograph of the high-altitude rocket ogive (fig. 10).

As the rocket Mach number increases, the shock approaches ogive nose. The transition from one flow pattern to another is gradual and continuous, provided that the Mach number does not change too rapidly.[2]

For a sphere in hypersonic flow at M = 10.77, the bow shock is detached, although close to the sphere.[3] Since the high-altitude rocket does not exceed Mach 3 for any portion of its trajectory, the bow shock will always remain detached throughout the flight regime.

---

[1] *D. W. Holder and A. Chinneck, The Flow Post Elliptic-Nosed Cylinders and Bodies of Revolution in Supersonic Air Streams, The Aeronautical Quarterly, IV (February 1954), 317-340.*

[2] *A. H. Shapiro, The Dynamics and Thermodynamics of Compressible Fluid Flow, II, New York, The Ronald Press Co. (1954), 88.*

[3] *Collane Tinkler, Hypersonic Flow, New York, Academic Press (1960), 65.*

Mach 1.5

p_{t_1} = 4 lb/in.^{2} abs

Mach 2.3

p_{t_1} = 50 lb/in.^{2} abs

Figure 10. Schlieren pictures showing flow pattern near ogive in wind tunnel (lb/in.^{2} abs × 6.894.7 = kPa).

The parameters needed to calculate the mass flow passing through the projectile are the fluid density and velocity in the vicinity of the stagnation region between the bow shock and the projectile. These parameters are obtained from normal shock tables[4] in terms of the free-stream conditions, and are shown in figure 11 for the high-altitude rocket ogive. The total pressure downstream of the normal shock is p_{t_2} and p_2 is the static pressure downstream of the normal shock.

[4] *Ames Research Staff, Equations, Tables and Charts for Compressible Flow, National Advisory Committee for Aeronautics, Report 1135, Moffet Field, CA (1953).*

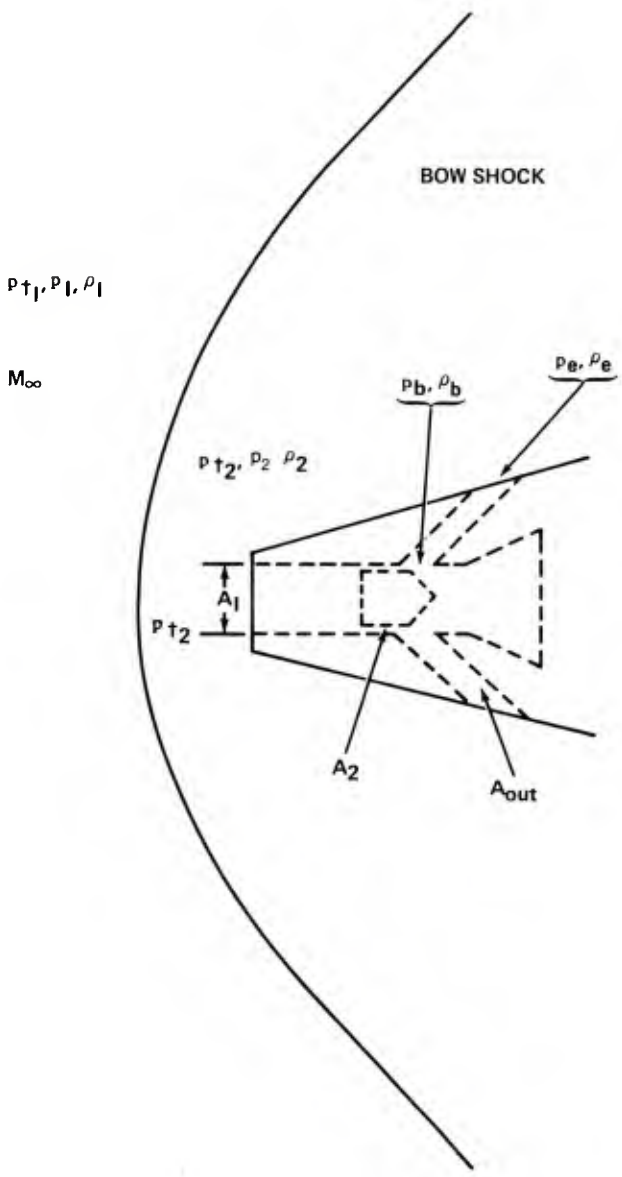

Figure 11. Supersonic flow pattern near ogive showing parameters for calculating mass flow rate.

An expression for the mass flow rate through the fluidic generator nozzle can be obtained as follows.

Consider a variable area duct (fig. 12) in which isentropic flow occurs. The mass flow rate is given in terms of the flow conditions at station (b), which corresponds to the annular nozzle in figure 11, by

$$\dot{m} = \rho_b \times A_b \times v_b \quad , \tag{1}$$

$$\left(\frac{\text{slug}}{\text{s}}\right) \quad \left(\frac{\text{slug}}{\text{ft}^3}\right) \quad (\text{ft}^2) \quad (\text{ft/s})$$

(1 slug = 14.59 kg, 1 ft = 0.3048 m)

where:

ρ_b is the static density,

A_b is the area of the fluidic generator annular nozzle, and

v_b is the velocity of air through the annular nozzle.

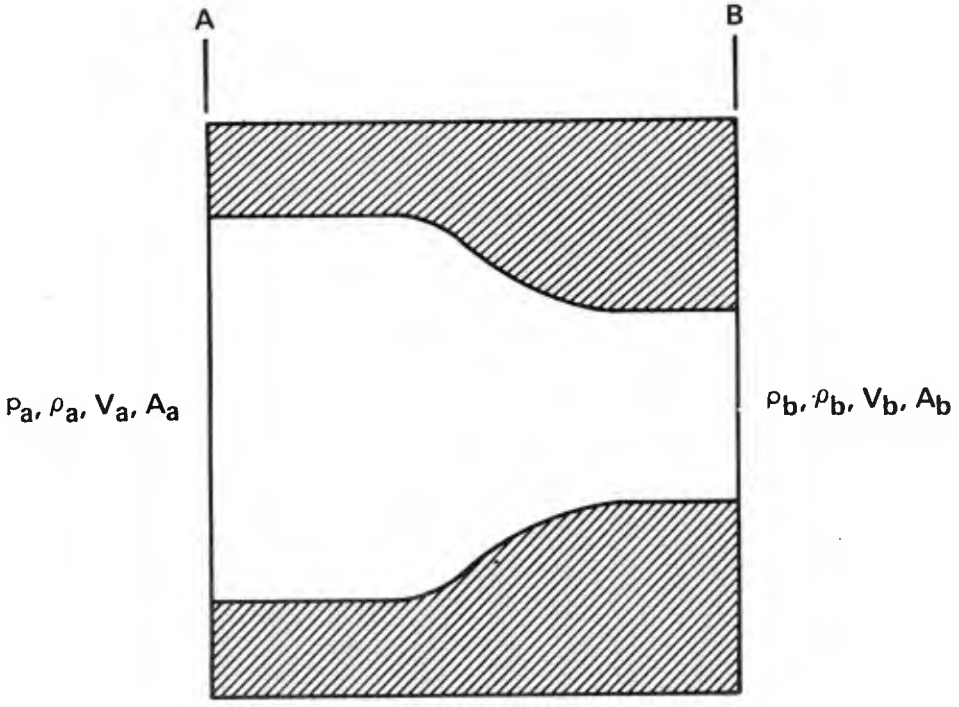

Figure 12. Flow conditions along streamline in variable area duct.

To express ρ_b and v_b in terms of the conditions at the entrance of the ogive (fig. 11), the right-hand side of equation (1) is multiplied and divided by ρ_a, C_a, and C_b.

$$\dot{m} = \left(\frac{\rho_b}{\rho_a}\right)\left(\frac{v_b}{C_b}\right)\left(\frac{C_b}{C_a}\right)\rho_a \; C_a \; A_b \quad . \tag{2}$$

In isentropic flow, the ratios in equation (2) may be expressed in terms of the pressure ratio $\left(p_b/p_a\right)$ by the following formulae from standard isentropic flow tables.

$$\frac{\rho_b}{\rho_a} = \left(\frac{p_b}{p_a}\right)^{\frac{1}{\gamma}} , \tag{3}$$

$$\frac{v_b}{C_b} \equiv M_b = \sqrt{\left(\frac{2}{\gamma-1}\right)\left[\left(\frac{p_b}{p_a}\right)^{-\left(\frac{\gamma-1}{\gamma}\right)} - 1\right]} \quad , \quad \text{and} \tag{4}$$

$$\frac{C_b}{C_a} = \left(\frac{p_b}{p_a}\right)^{\frac{\gamma-1}{2\gamma}} , \tag{5}$$

where $\gamma = 1.4$ is the ratio of specific heat capacities for air.

These relationships can be substituted into equation (2) to furnish the following expression for mass flow through the fluidic generator in terms of the pressures across the annular nozzle and the area of the annular nozzle.

$$\underset{\left(\frac{\text{slug}}{\text{s}}\right)}{\dot{m}} = \left(\frac{p_b}{p_a}\right)^{\frac{\gamma+1}{2\gamma}} \sqrt{\left(\frac{2}{\gamma-1}\right)\left[\left(\frac{p_b}{p_a}\right)^{-\left(\frac{\gamma-1}{\gamma}\right)} - 1\right]} \; \underset{\left(\frac{\text{slug}}{\text{ft}^3}\right)\left(\frac{\text{ft}}{\text{s}}\right)\left(\text{ft}^2\right)}{\rho_a \quad C_a \quad A_b} \quad . \tag{6a}$$

In terms of laboratory units, this equation is

$$\dot{m}_{(SCFM)} = 175.215 \left(\frac{p_b}{p_a}\right)^{\frac{\gamma+1}{2\gamma}} \sqrt{\left(\frac{2}{\gamma-1}\right)\left[\left(\frac{p_b}{p_a}\right)^{-\left(\frac{\gamma-1}{\gamma}\right)} - 1\right]} \quad \rho_a \; C_a \; A_b \quad \cdot \quad (6b)$$

$$\left(\frac{\text{slug}}{\text{ft}^3}\right)\left(\frac{\text{ft}}{\text{s}}\right)(\text{in.}^2)$$

(1 SCFM = 577 × 10^{-6} kg/s)

For pressure ratios $\frac{p_b}{p_a} \leq 0.5283$,

the flow in the annular nozzle is choked, and further reduction in the pressure P_b has no effect on the mass flow rate, which then depends only on the inlet conditions. The mass flow rate for choked flow is given by substituting $p_b/p_a = 0.5283$ into equation (6b), or

$$\dot{m}_{(SCFM)} = 101.4 \times \rho_a \times C_a \times A_b \qquad (7)$$

$$\left(\frac{\text{slug}}{\text{ft}^3}\right)\left(\frac{\text{ft}}{\text{s}}\right)(\text{in.}^2)$$

3.2.2 Calculation of Mass Flow Rate in Laboratory

In the laboratory apparatus shown in figure 8, the total pressure, p_{sup}, in the settling chamber is the pressure p_a at the generator inlet (eq 6). The exhaust port conditions are p_∞, ρ_∞, and C_∞. Since the exhaust port area is larger than the nozzle area, the values of pressure and density at the nozzle (p_b and ρ_b) are assumed to be equal to the ambient conditions ($p_E = p_\infty$, $\rho_E = \rho_\infty$) at the exhaust. Hence, equations (6) and (7) become, for the laboratory apparatus,

$$\dot{m}_{\substack{LAB \\ (SCFM)}} = \begin{cases} 175.215 \left(\frac{p_\infty}{p_{sup}}\right)^{\frac{\gamma+1}{2\gamma}} \sqrt{\left(\frac{2}{\gamma-1}\right)\left[\left(\frac{p_\infty}{p_{sup}}\right)^{-\left(\frac{\gamma-1}{\gamma}\right)} - 1\right]}\ \rho_{sup}\ C_{sup}\ A_b & \text{for } \frac{p_\infty}{p_{sup}} > 0.5283 \\ 101.4 \left(\rho_{sup}\ C_{sup}\ A_b\right) & \text{for } \frac{p_\infty}{p_{sup}} \leq 0.5283 \end{cases} . \quad (8)$$

For the laboratory,

$$\rho_{sup} = \frac{p_{sup}}{p_\infty}\ \rho_\infty , \quad \text{and} \quad C_{sup} = \sqrt{\frac{\gamma p_{sup}}{\rho_{sup}}} , \quad \text{and } C_\infty = \sqrt{\frac{\gamma p_\infty}{\rho_\infty}}$$

$$\text{so that } \rho_{sup}\ C_{sup} = \frac{\gamma}{C_\infty}\ p_{sup} . \quad (9)$$

The mass flow rate in the laboratory calculated from equations (8) and (9) using the values

$$\begin{aligned} A_b &= 0.068 \text{ in.}^2 \ (43.8 \times 10^{-6} \text{ m}^2), \\ \rho_\infty &= 0.002378 \text{ slugs/ft}^3 \ (1.225 \text{ kg/m}^3), \\ p_\infty &= 14.7 \text{ lb/in.}^2 \text{ abs } (101.35 \text{ kPa}), \\ C_\infty &= 1117 \text{ ft/s } (340.46 \text{ m/s}), \text{ and} \\ \gamma &= 1.4 \end{aligned} \quad (10)$$

is compared with measured values in figure 13. This shows that the theoretical model can be used to calculate the mass flow rate through the fluidic generator in the laboratory.

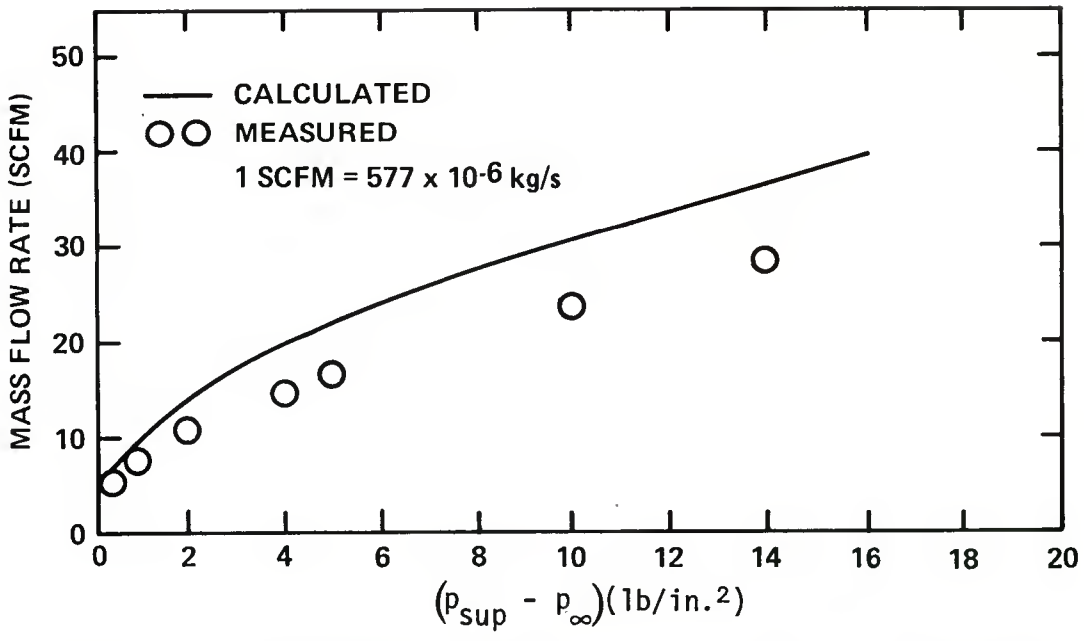

Figure 13. Comparison of measured and calculated mass flow rate to fluidic generator in laboratory.

3.2.3 Calculation of Mass Flow Rate in Wind Tunnel

In the wind tunnel, the pressure p_a in equation (6) is the total pressure p_{t_2} downstream of the bow shock (fig. 11). The pressure p_E at the exhaust ports depends on the air properties and the ogive shape. Hence, the pressure is not known exactly. As in the laboratory case, p_E is assumed to be equal to the pressure p_b at the annular nozzle. For the condition of choked flow through the nozzle, p_E does not affect the mass flow rate.

For the supersonic flow regime investigated in this wind tunnel test, the choked flow equation for the mass flow rate is

$$\dot{m} = 101.4 \times \rho_{t_2} \times C_{t_2} \times A_b \qquad (11)$$

$$(\text{SCFM}) \qquad \left(\frac{\text{slug}}{\text{ft}^3}\right)\left(\frac{\text{ft}}{\text{s}}\right)\left(\text{in.}^2\right)$$

The term $(\rho_{t2}\ C_{t2})$ for stagnation conditions downstream of the bow shock can be evaluated in terms of the free-stream conditions, M_1, p_{t_1}, and T_{t_1} (temperature) by

$$\rho_{t_2}\ C_{t_2} = \sqrt{\frac{144\gamma}{R}\ \frac{\left(\frac{\rho_1}{\rho_{t_1}}\right)\left(\frac{\rho_2}{\rho_1}\right)\left(\frac{p_{t_2}}{p_{t_1}}\right)}{\left(\frac{\rho_2}{\rho_{t_2}}\right)}\ p_{t_1} \times \rho_{t_1}} \tag{12}$$

$$\left(\frac{\text{slug}}{\text{s} \cdot \text{ft}^2}\right) \qquad (\text{lb/in.}^2\ \text{abs}) \left(\frac{\text{slugs}}{\text{ft}^3}\right)$$

where

$$\rho_{t_1} = \frac{p_{t_1}}{RT_{t_1}} \tag{13a}$$

and

$$\frac{\rho_2}{\rho_{t_2}} = \left(1 + 0.2M_2^{\,2}\right)^{-\frac{5}{2}}, \quad R = 1716\ \frac{\text{ft}^2}{\text{s}^2 \cdot {}^\circ\text{R}}\ \text{, gas constant.} \tag{13b}$$

Substituting (13) into (12) gives

$$\rho_{t_2}\ C_{t_2} = \sqrt{\frac{144\gamma}{R}\ \frac{\left(\frac{\rho_1}{\rho_{t_1}}\right)\left(\frac{\rho_2}{\rho_1}\right)\left(\frac{p_{t_2}}{p_{t_1}}\right)}{\left(\frac{\rho_2}{\rho_{t_2}}\right)}\ \frac{p_{t_1}^2}{T_{t_1}}}\ . \tag{14}$$

The above ratios, including M_2, are available from isentropic flow tables in terms of M_1.

3.2.4 Calculation of Mass Flow Rate for Flight

For estimating mass flow rate for flight conditions, the given variables are usually free-stream Mach number and altitude. Atmospheric pressure and speed of sound can be obtained in terms of altitude from standard atmospheric tables.

Equation (14) can be expressed in terms of atmospheric conditions by

$$\rho_{t_2} C_{t_2} = \frac{\gamma p_1 (\mathrm{lb/ft^2})}{C_1 (\mathrm{ft/s})} \times \sqrt{\left(\frac{p_1}{p_{t_2}}\right)^{-1} \left(\frac{\rho_2}{\rho_{t_2}}\right)^{-1} \left(\frac{\rho_2}{\rho_1}\right)} \qquad (15)$$

where the ratios p_1/p_{t2} and ρ_2/ρ_1, and M_2 are obtained from the isentropic flow tables. The ratio ρ_2/ρ_{t_2} is obtained in terms of M_2 from equation (13b).

Thus, the mass flow rate formula for choked flow for flight conditions is equation (11), with $(\rho_{t_2} C_{t_2})$ given by equations (15) and (13b).

3.3 Method of Estimating Generator Voltage in Wind Tunnel or in Flight

The apparatus shown in figure 8 was used to measure the voltage supplied by the fluidic generator to a 2.5-kohm load versus mass flow rate. A laboratory calibration curve was then plotted from the data, as shown in figure 14. In this curve both the output voltage and supply mass flow rate are measured quantities. The mass flow rate can be calculated for given wind tunnel or flight conditions by the methods of section 3.2. The voltage corresponding to each value of mass flow rate then can be obtained from the calibration curve.

This was done for the measured conditions of total pressure and total temperature in the wind tunnel at Mach 1.5. The mass flow rates corresponding to the tunnel data were calculated and the expected voltages were obtained from figure 14. The expected voltage is compared with the voltage measured in the wind tunnel in figure 15. The agreement is exact.

A close estimate of the voltage also can be obtained by using the properties of the standard atmosphere instead of the total temperature measured in the tunnel. In figure 16, the mass flow rate is calculated for wind tunnel runs at Mach 1.5, 1.76, and 2.02.

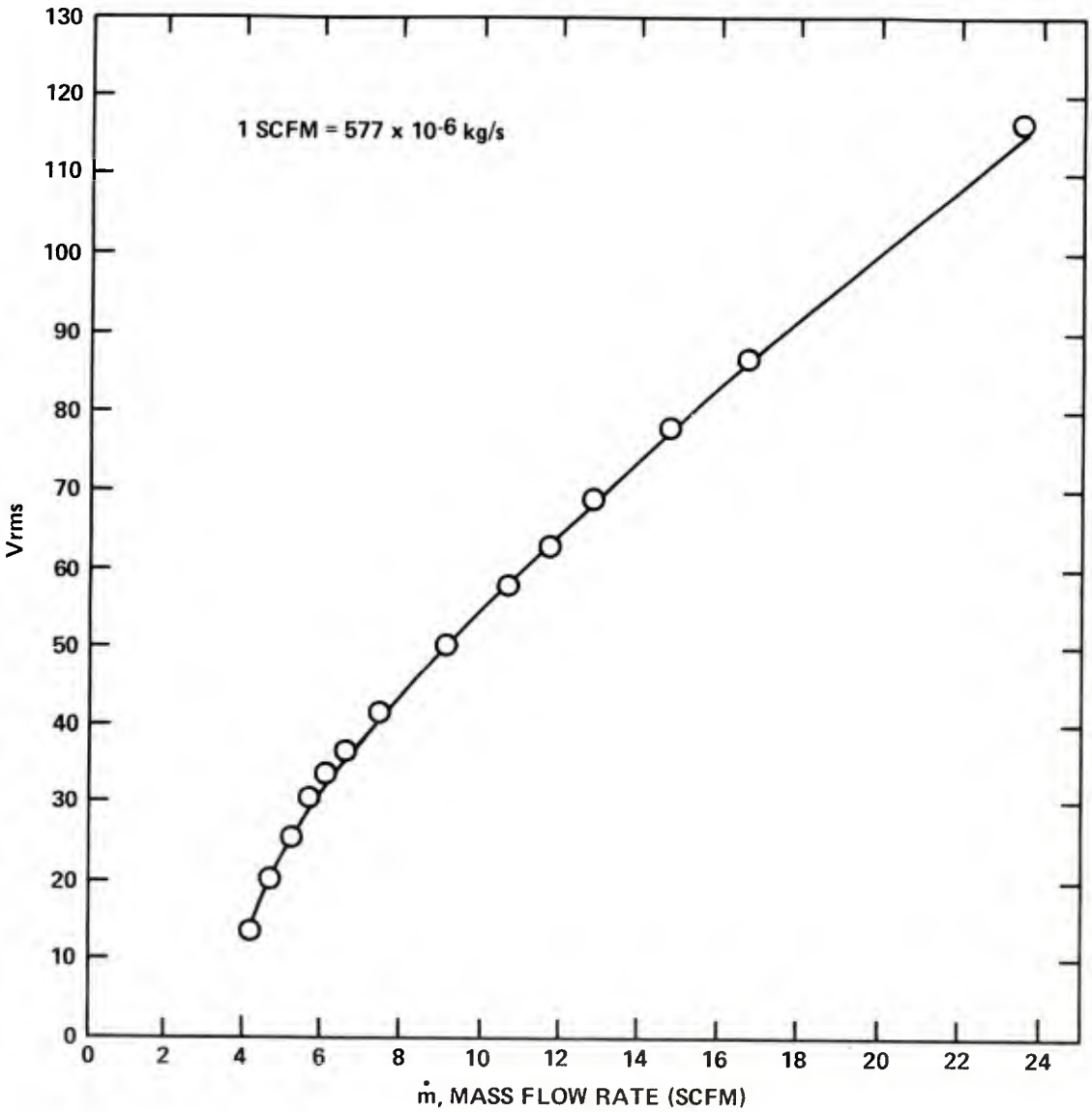

Figure 14. Laboratory calibration curve for fluidic generator.

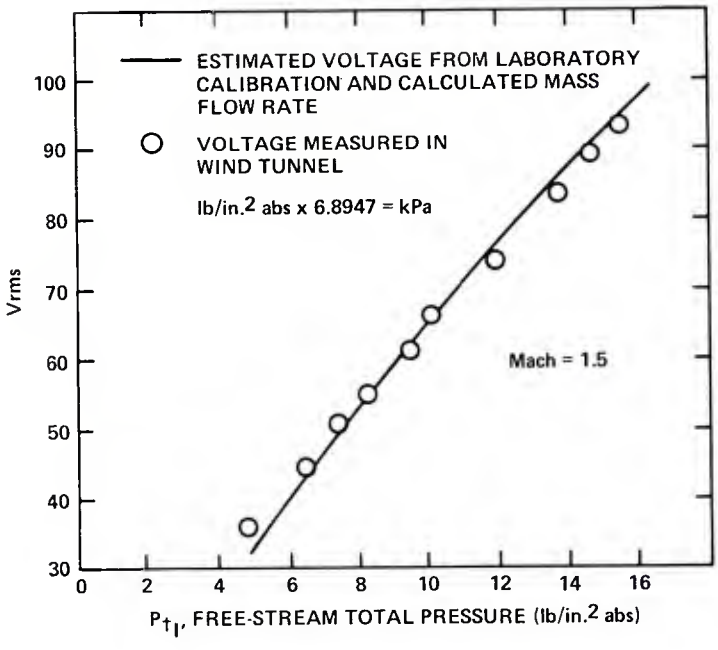

Figure 15. Comparison of expected generator voltage measured in wind tunnel at M = 1.5.

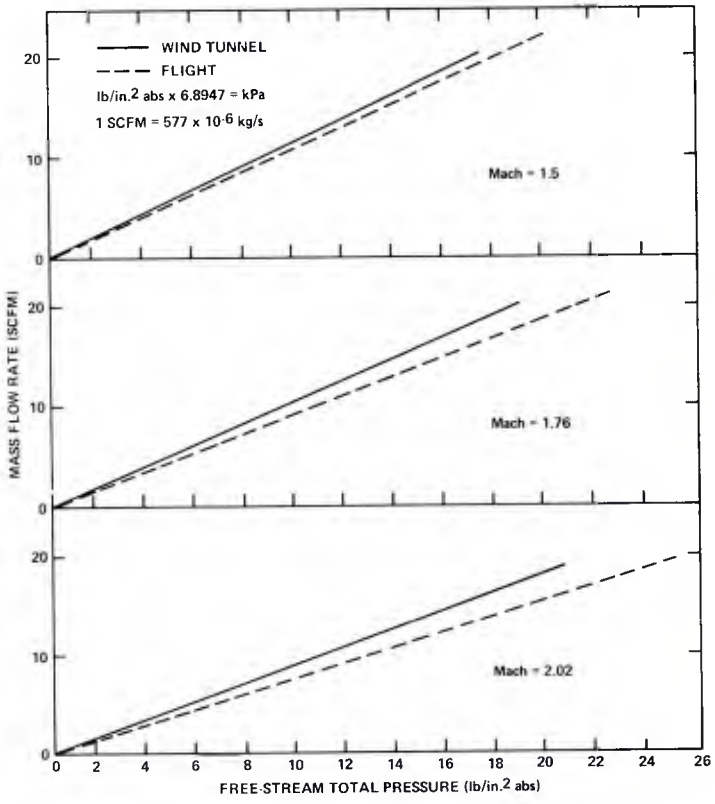

Figure 16. Comparison of mass flow rate calculated using flight and wind tunnel conditions.

The first mass flow rate calculations used the measured total temperature values for each given Mach number and total pressure. The calculations were then repeated using the temperature of the standard atmosphere, which would be encountered in an ideal flight. Slightly lower mass flow rates are obtained by using the atmospheric conditions. Consequently, slightly lower voltages would be estimated from the calibration curve of figure 14. Figure 16 shows the closeness of the wind tunnel conditions to flight conditions in determining the mass flow rate to the fluidic generator. Thus, the laboratory calibration with the method of calculating the mass flow rate can be used to estimate the generator output under specified flight conditions.

This method was developed for use at conditions near the apex of the high-altitude trajectories, where the mass flow rate available to the generator is a minimum, and where the flow pattern contains a bow shock as shown in figure 11.

3.4 Comparison of Expected Voltage with Voltage Observed in Wind Tunnel at Higher Mach Numbers

The flow pattern shown schematically in figure 11 is closely approximated by the actual flow pattern at Mach 1.5 (fig. 10a). At higher Mach numbers, for example, Mach 2.3 in figure 10b, additional shocks are formed at the exhaust ports, so that the assumptions made regarding the exhaust port pressure are no longer valid. Nevertheless, it is possible to use the model to estimate the output at the higher Mach numbers, although accuracy is reduced.

The model has been used in figures 17 and 18 for the higher Mach number data from the wind tunnel. The expected and measured generator voltages for the wind tunnel are plotted versus free-stream total pressure for Mach numbers of 1.76 and 2.02 in figures 17 and 18, respectively.

3.5 Conclusions Concerning Method for Predicting Generator Output

A method has been developed that uses laboratory calibration of generator output versus supply pressure and mass flow, together with calculated mass flow values along flight trajectories, to predict the generator voltage for either flight or wind tunnel conditions near the apex of the high-altitude trajectory, where the pneumatic input power to the fluidic generator is a minimum. The method has been verified in the wind tunnel up to Mach 2.02 and free-stream total pressures up to 20 $lb/in.^2$ abs (137 kPa). The method can be used to predict the least expected output in flight, so that actual values obtained will be higher over the same pressure range. The method is best at low free-stream total pressures where the assumptions used in the calculations are most valid, and the generator output can be verified in the laboratory.

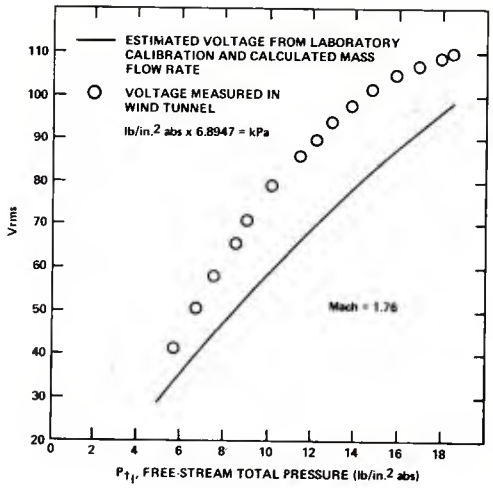

Figure 17. Comparison of expected generator voltage with values measured in wind tunnel at M = 1.76.

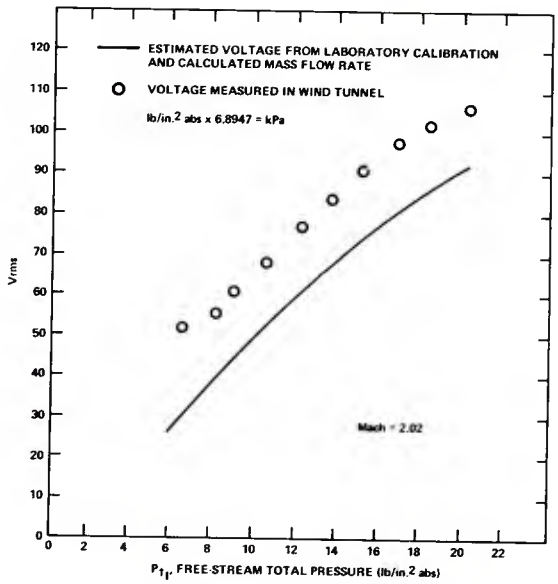

Figure 18. Comparison of expected generator voltage with values measured in wind tunnel at M = 2.02.

4. SUMMARY OF WIND TUNNEL TEST RESULTS

Wind tunnel tests conducted at NSWC on 19 and 20 July 1977 furnished information on fluidic generator output near the apex of the worst-case trajectory of a proposed high-altitude rocket. These tests provided data that were used to relate laboratory calibration data to generator output in flight.

The wind tunnel data corresponding to points on the worst-case trajectory have shown that the fluidic generator operated throughout the test. The generator output voltage was a minimum near the apex where available pneumatic power is low.

The wind tunnel was used to verify a method of predicting the fluidic generator voltage in flight, given a laboratory calibration curve of generator output as a function of supply mass flow rate. The method developed includes a theoretical model for calculating the mass flow through the generator in flight or in the wind tunnel. The voltages estimated by using the calibration curve, and the mass flows calculated for the expected flight conditions, furnished a low estimate of the output, when compared with voltages measured in the wind tunnel. The method was verified for Mach numbers up to 2.02 and free-stream total pressures up to 20 $lb/in.^2$ abs (137 kPa). The method is especially accurate for the conditions near the apex of the high-altitude trajectory where the mass flow available to the generator is a minimum. The latter condition was most desirable for the development of the generator.

Limitations in accuracy at the higher Mach numbers result from the assumptions in the mass flow calculations, which are less accurate at higher Mach numbers. The generator configuration used in the wind tunnel was fired aboard 5-in. rockets for low-altitude testing. The results of that test can be found in the GSRS-1 (General Support Rocket System) field test summary (3 October 1977, Memorandum from Carl J. Campagnuolo to R. Goodman, HDL).

LITERATURE CITED

(1) D. W. Holder and A. Chinneck, The Flow Post Elliptic-Nosed Cylinders and Bodies of Revolution in Supersonic Air Streams, The Aeronautical Quarterly, IV (February 1954), 317-340

(2) A. H. Shapiro, The Dynamics and Thermodynamics of Compressible Fluid Flow, II, New York, The Ronal Press Co. (1954), 88.

(3) Collane Tinkler, Hypersonic Flow, New York, Academic Press (1960), 65.

(4) Ames Research Staff, Equations, Tables and Charts for Compressible Flow, National Advisory Committee for Aeronautics, Report 1135, Moffet Field, CA (1953).

ACKNOWLEDGEMENTS

The author wishes to acknowledge the assistance and contributions of the following people: Henry C. Lee, who provided the generators and calibration in data for the test, Michael Salyards and LeRoy Hughes, who assisted in gathering and reducing the wind tunnel data, and Carl Campagnuolo for his invaluable guidance on the theoretical model.

Further, the cooperation of the Naval Surface Weapons Center supersonic wind tunnel staff in accomplishing the test objectives is appreciated, especially the assistance of John Holmes and Joseph Knott.

DISTRIBUTION

ADMINISTRATOR
DEFENSE DOCUMENTATION CENTER
ATTN DDC-TCA (12 COPIES)
CAMERON STATION, BUILDING 5
ALEXANDRIA, VA 22314

COMMANDER
US ARMY RSCH & STD GP (EUR)
ATTN LTC JAMES M. KENNEDY, JR.
CHIEF, PHYSICS & MATH BRANCH
FPO NEW YORK 09510

COMMANDER
US ARMY MATERIEL DEVELOPMENT &
READINESS COMMAND
ATTN DRXAM-TL, HQ TECH LIBRARY
5001 EISENHOWER AVENUE
ALEXANDRIA, VA 22333

COMMANDER
US ARMY ARMAMENT MATERIEL
READINESS COMMAND
ATTN DRSAR-ASF, FUZE &
MUNITIONS SUPPORT DIV
ATTN DRSAR-LEP-L, TECHNICAL LIBRARY
ROCK ISLAND, IL 61299

COMMANDER
US ARMY MISSILE & MUNITIONS
CENTER & SCHOOL
ATTN ATSK-CTD-F
REDSTONE ARSENAL, AL 35809

DIRECTOR
US ARMY MATERIEL SYSTEMS
ANALYSIS ACTIVITY
ATTN DRXSY-MP
ABERDEEN PROVING GROUND, MD 21005

DIRECTOR
US ARMY BALLISTIC RESEARCH LABORATORY
ATTN DRDAR-TSB-S (STINFO)
ABERDEEN PROVING GROUND, MD 21005

COMMANDER
US ARMY MISSILE RES & DEV COMMAND
REDSTONE ARSENAL, AL 35809
ATTN DRCPM-RS, GEN SPT ROCKET SYS
ATTN DRCPM-RK, 2.75 INCH ROCKET SYS
ATTN DRCPM-RSE, H. PORTER
ATTN DRCPM-RSE, B. RICHARDSON

COMMANDER
NAVAL SURFACE WEAPONS CENTER
WHITE OAK, MD 20910
ATTN WX-40, TECHNICAL LIB
ATTN K81, J. HOLMES
ATTN K81, J. KNOTT

US ARMY ELECTRONICS RESEARCH
& DEVELOPMENT COMMAND
ATTN WISEMAN, ROBERT S., DR., DRDEL-CT
ATTN PAO

HARRY DIAMOND LABORATORIES
ATTN 00100, COMMANDER/TECHNICAL DIR/TSO
ATTN CHIEF, 00210
ATTN CHIEF, DIV 10000
ATTN CHIEF, DIV 20000
ATTN CHIEF, DIV 30000
ATTN CHIEF, DIV 40000
ATTN CHIEF, LAB 11000
ATTN CHIEF, LAB 13000
ATTN CHIEF, LAB 15000
ATTN CHIEF, LAB 22000
ATTN CHIEF, LAB 21000
ATTN CHIEF, LAB 34000
ATTN CHIEF, LAB 36000
ATTN CHIEF, LAB 47000
ATTN CHIEF, LAB 48000
ATTN RECORD COPY, 94100
ATTN HDL LIBRARY, 41000 (5 COPIES)
ATTN HDL LIBRARY, 41000 (WOODBRIDGE)
ATTN CHAIRMAN, EDITORIAL COMMITTEE
ATTN TECHNICAL REPORTS BRANCH, 41300
ATTN LEGAL OFFICE, 97000
ATTN LANHAM, C., 00210
ATTN WILLIS, B., 47400
ATTN CHIEF, BR 34400
ATTN CHIEF, BR 34200
ATTN CHIEF, BR 34600
ATTN BEARD, J., 34600
ATTN CROARKIN, J., 34400
ATTN FINGER, D., 34400
ATTN CAMPAGNUOLO, C., 34600
ATTN DAVIS, H., 34600
ATTN CHIEF, BR 13400
ATTN GEHMAN, S., 13400
ATTN LEE, H., 34600
ATTN SALYARDS, M., 34600
ATTN FINE J., (20 COPIES)